
Article:
Peng, Z., Stovin, V. and Guymer, I. orcid.org/0000-0002-1425-5093 (2024) Radial mixing in steady and accelerating pipe flows. ASCE Journal of Hydraulic Engineering, 150 (6). ISSN 0733-9429

https://doi.org/10.1061/JHEND8.HYENG-14071

Radial Mixing in Steady and Accelerating Pipe Flows

Zhangjie Peng [1], Virginia Stovin[2] and Ian Guymer[3]

[1]Research Associate, Department of Civil and Structural Engineering, The University of Sheffield, Mappin Street, Sheffield, S1 3JD, United Kingdom. Email: zhangjie.peng@sheffield.ac.uk

[2]Professor of Green Infrastructure for Stormwater Management, Department of Civil and Structural Engineering, The University of Sheffield, Mappin Street, Sheffield, S1 3JD, United Kingdom. Email: v.stovin@sheffield.ac.uk

[3]Professor of Civil Engineering, Department of Civil and Structural Engineering, The University of Sheffield, Mappin Street, Sheffield, S1 3JD, United Kingdom. Email: i.guymer@sheffield.ac.uk

ABSTRACT

Understanding solute transport in pipe flows is essential for ensuring consistent water quality throughout the entire drinking water supply network. This study utilised four Planar Laser-Induced Fluorescence (PLIF) units for the first time to quantify the cross-sectional concentration distribution resulting from a single pulse of tracer injected at an upstream location under both steady and accelerating flow conditions. In comparison with conventional fluorometers, PLIF provides a better measure of the cross-sectional mean concentrations, because it allows the cross-sectional distribution of the tracer to be quantified. Under steady turbulent flow conditions, the tracer was cross-sectionally well-mixed, and the concentration uniformity increased with increasing Reynolds number. In laminar flows, as a result of minimal radial mixing, the tracer exhibited a spatial distribution created by the longitudinal differential advection, transforming from a central core to an annulus, which expanded towards the pipe boundary. Under accelerating flows, the temporal concentration profiles displayed two peaks and the tracer close to the source was not cross-sectionally well-mixed. With increasing discharge, the tracer became cross-

sectionally well-mixed while retaining the two peak profiles. These results have implications for water quality modelling in unsteady conditions, especially in domestic plumbing, when boundary and biofilm interactions control important processes.

Keywords: Solute Transport; Steady; Unsteady; Pipe Flow; Concentration Distribution.

INTRODUCTION

Understanding solute transport in drinking water distribution networks is key to maintaining consistent water quality throughout the networks. The ability to accurately model the peak concentration and longitudinal spread of disinfectants or accidentally introduced contaminants in the network is critical for protecting public health (Piazza *et al*., 2020, Lee e*t al*., 2023). In main drinking water distribution networks, the flow condition is typically considered to be steady turbulent flow, in which advection outweighs the impact of longitudinal dispersion. Many water quality models for distribution networks assume turbulent flow conditions, and only model bulk advection, neglecting longitudinal dispersion (Rossman, 2000; Romero-Gomez and Choi, 2011). However, in peripheral regions, where water leaves the main network and enters the customers' consumption points, laminar and transitional flow conditions exist in the pipe (Buchberger *et al*., 2003; Shang *et al*., 2023). In premises plumbing systems, flow conditions tend to be laminar for much longer periods, increasing water quality concerns due to the risks associated with human exposure to contaminants (Lee *et al*., 2023).

In a distribution network, flow is not steady. Various factors, such as pump stoppage, sudden changes in local intermittent demand, or the opening and closing of valves, can lead to periods of unsteady discharge in all parts of the network (Hart *et al*., 2021; LeChevallier *et al*., 2003). Experimental studies on unsteady flows have focused on measuring temporal local mean radial velocity profiles at a single location (Greenblatt and Moss, 2004; He and Jackson, 2000; Kurokawa and Morikawa, 1986). However, these measurements lack the short-term, temporal turbulent velocity fluctuations across

pipe radius during the unsteady flows that are needed to quantify the local radial mixing characteristics. Therefore, there is a pressing need for an understanding and improved modelling of how contaminants travel and spread in unsteady flow scenarios (Burkhardt *et al*., 2020; Shang *et al*., 2023, Lee *et al*., 2023).

Solute tracers used to determine longitudinal dispersion are required to be easy to detect and have similar physical properties to water. Fluorescent tracers serve this purpose well as they are mostly conservative, have a low limit of detection, and are used extensively in various applications (Swarnkar *et al*., 2022; Wilson *et al*., 1986). Fluorometers are devices to measure fluorescent tracer concentrations. The Turner Designs Series 10 fluorometer (Turner Designs, San Jose, California) is designed to take static cuvette samples and dynamic flow-through measurements. Hart *et al*. (2016, 2021) employed a number of these fluorometers, with a 24 mm internal diameter perspex pipe passing through, for nonintrusive concentration measurements under different steady and unsteady flow conditions. These fluorometers output a single concentration value at each time step, and in their analysis, the authors treated this value as the cross-sectional area mean concentration. However, in laminar flows, the tracer is usually not perfectly cross-sectionally well-mixed, and such measurements may not accurately represent the cross-sectional area mean concentrations at these conditions.

Laser Induced Fluorescence (LIF) is a nonintrusive measurement technique based on optical principles used for qualitative and quantitative descriptions of flow and mixing phenomena. van Cruyningen *et al.* (1990) demonstrated that it was possible to use laser light-sheets as an illumination source for fluorescent dye concentration measurements. Harry *et al.* (1996) developed an in-situ concentration measurement technique to investigate vertical mixing processes in a laboratory representation of the coastal zone. A typical LIF system consists of an illumination source (laser), fluorescent compounds, image acquisition devices (camera) and illumination optics (Crimaldi, 2008). With the aid of optics, a light sheet can be generated to illuminate a plane area. Planar Laser-Induced Fluorescence (PLIF) offers the opportunity to measure 2D (cross-sectional) concentration distributions, which can also be used to determine an accurate pipe cross-sectional mean concentration. To date, no study has

attempted to employ PLIF to measure 2D concentration distributions at multiple locations for pipe flows.

When a solute or contaminant is introduced into pipe flow, it disperses in all directions. Longitudinal dispersion is caused by the combined effects of cross-sectional differential advection and radial diffusion. For a pulse of contaminant, this changes the area mean temporal solute concentration profile as it travels along the flow direction, reducing the peak concentration and increasing the spread. Studies on pipe mixing have focused on quantifying longitudinal dispersion under different steady flow conditions using measured tracer temporal cross-sectional mean concentration profiles at different downstream locations (Fowler and Brown, 1943; Taylor, 1954; Flint and Eisenklam, 1969; Keyes, 1955; Hart *et al*., 2016; Piazza *et al*., 2020). In these studies, the tracer concentration was measured either at the pipe wall, through tapping points, at the discharge point or non-invasively by fluorometers at different downstream locations along the pipe. These measurements lead to a 1D concentration measurement, often assumed to be the cross-sectional mean value. No study has directly measured 2D spatial distributions over the pipe cross-section.

Pipe flows can be categorised into laminar, transitional, and turbulent flow, each exhibiting distinct mixing characteristics. Laminar flow is characterised by streamline motion, where the only velocity component is longitudinal, and the radial exchange is due to molecular diffusion. This generates high values of longitudinal dispersion, D_x (m^2/s), with the dimensionless longitudinal dispersion coefficient, $D_x^* = D_x/\bar{u}d$, of around 20 at Re = 2,000, where $\bar{u}$ = cross-sectional mean velocity and d = pipe internal diameter. In turbulent flow, rapid local velocity fluctuations promote radial mixing, leading to lower longitudinal dispersion, with D_x* of around 0.4 at Re = 50,000 (Hart *et al*., 2016). Transitional flow represents a condition where either laminar or turbulent flow can occur (Mathieu and Scott, 2000).

Hart *et al.* (2021) investigated longitudinal dispersion in unsteady pipe flows. Both accelerating and decelerating flow cases were studied, within the turbulent flow range and between laminar and

turbulent flow conditions. In most cases, the 1D concentration measured by the fluorometers revealed single peaked distributions at each location. The exception was during acceleration from laminar to turbulent flow conditions when a previously unreported disaggregation of the single 1D tracer cloud was observed. This is illustrated in Fig. 1, where the upstream temporal concentration profile, recorded during flows with Re ≈ 3,500, exhibited a single peak distribution, following the expected Gaussian form of distribution. Once this single pulse of tracer experienced accelerating flows, upto Re ≈ 8,000, it was shown to disaggregate into multiple pulses over the following ~2 m length of pipe.

Insert Fig. 1

The mechanism responsible for creating the observed disaggregation was not identified, as measurements were limited by the 1D area mean concentrations and the lack of hydrodynamic measurements. Hence, as a first step to understand the physical processes, this paper presents novel measurements to explore the temporal variation of cross-sectional tracer distribution (tracer uniformity) in pipe flows accelerating from laminar to turbulent conditions. The objectives of this study are to:

1. Quantify the limitations of using 1D fluorometers for determining area mean concentration;
2. Visualise pipe 2D spatial and temporal tracer concentration distributions under steady and accelerating flows;
3. Quantify the degree of tracer uniformity over the pipe cross section during these conditions.

MATERIALS AND METHODS

Experimental Rig

Experiments were conducted on a section of 13 m long, 24 mm internal diameter perspex pipe (Fig. 2(a)). This test section was connected to a recirculating system, with water from a ground-level sump (3 m^3) pumped to a 1 m^3 header tank 10 m above, before entering the test section. To maintain a constant water head, an overflow pipe was installed on the upper tank. A perspex plate (inlet in Fig.

2(a)) with an opening of 4.75 mm was placed before the test section to reduce the flow rate within the test section. Flow control was achieved with a digital butterfly valve (Series J3C, J+J Deutschland GmbH, Germany) located at the end of the test section.

During the experiment, a fluorescent tracer, Rhodamine 6G, was injected into the flow from the pipe wall using a pressurised vessel equipped with a solenoid valve. The injection point was 2.043 m downstream from the start of the test section, a length considered sufficient for flow to be fully developed. The pressure vessel maintained a constant pressure of 2.0 bar, and the computer-controlled solenoid valve ensured consistent injected tracer volume and timing. The injection pressure used in this study is to ensure a cross-sectional well-mixed condition at the injection point and minimise the influence of injection on the downstream concentration distributions. Fig. 2(b) visualises the dye distribution near the injection location after the injection using a red food dye, the dye was cross-sectionally well-mixed at the first few centimetres downstream of the injection location.

The discharge from the pipe was determined from a calibrated differential pressure transducer (PD33X, KELLER, Switzerland) across a 7 mm diameter orifice. The relationship between the differential pressure transducer output, digital butterfly valve opening and the discharge was calibrated using volumetric measurements of discharge. Two tapping points were made on the pipe, 11.779 m apart, for measuring the pipe head loss with a calibrated differential pressure transducer (PXM409-025HDWUI, OMEGA Engineering, USA).

To ensure that the most of tracer passed all the measurement locations during the accelerating flow zone, instruments were placed within 6 m downstream of the injection location. Four Turner Designs Series 10 fluorometers, F1 to F4 (Turner Designs, San Jose, USA) were placed downstream of the injection point to non-intrusively measure the temporal concentration profiles. The pipe passed through the fluorometers, and all the outside sections were covered with black sheets to prevent the interference of external light. Four Planar Laser-Induced Fluorescence (PLIF1 to PLIF4) units were

placed immediately downstream of the fluorometers to measure the cross-sectional concentration distributions.

Fig. 2(c) details the design for the PLIF unit used in this study. The unit consists of a water bath, laser beam, optics and a camera. The pipe passed through the sealed water bath to minimise refraction. A 220 mW laser beam, with a wavelength of 532 nm, was used along with a Powell lens and a collimator to generate a vertical laser sheet, illuminating the cross-section of the pipe in the water bath through the glass window at 90° to the direction of flow. A camera (FL3-U3-13Y3M-C, FLIR, USA) was mounted at 45° to the flow direction, capturing the pipe's cross-sectional images through a glass window on the water bath. A long-pass filter (530 nm) was fitted to the camera lens to cut out the laser light. The camera was connected to the computer and controlled through MATLAB (MathWorks Inc., R2022a). The camera parameters were established through initial tests to ensure that, at all locations, the maximum concentration occurring in the pipe was within the image scale. All the components were fixed on a plate, and the entire unit was covered with a black lid to avoid any influence of external light.

Insert Fig. 2.

PLIF and Fluorometer Calibration

As the camera in the PLIF unit is 45° to the flow direction, the raw image taken for the circular pipe cross-section appears as an oval shape. Image correction was performed to convert the oval shape to a circle and establish a relationship between image coordinates and real-world coordinates. A 24 mm diameter circle target with a checkerboard pattern of 4 mm squares was inserted into the pipe section for reference images. The images were processed in MATLAB (MathWorks Inc., R2022a) to establish the conversion relationships. Detailed descriptions of the image correction can be found in Supplementary Material A.

The direct output from the fluorometers is voltage, and calibrations were performed to determine the relationship between tracer concentration and output voltage. The vertical laser sheet generated by the laser and optics in the PLIF unit is not perfectly uniform, and the calibration with PLIF involves correcting the vertical laser sheet intensity uniformity and converting greyscale image intensity to tracer concentration. Details on the fluorometers and PLIF calibration can be found in Supplementary Material B.

Test Programme

Headloss measurements were carried out to characterise the pipe hydraulics. Subsequently, temporal concentration profiles and cross-sectional concentration distributions were measured during a series of steady flow conditions and a single accelerating flow condition.

Headloss measurements were conducted under 42 steady conditions, covering Reynolds numbers ranging from 700 to 11,000. For each steady flow condition, discharge and headloss were recorded for a duration of 210 s at a frequency of 100 Hz. The mean discharge during this period was then converted to Reynolds number using the viscosity corresponding to the measured water temperature in the pipe, and the friction factor was calculated based on the average head loss using Eq. 1

$$f = h_f\left(\frac{d}{L}\right)\left(\frac{2g}{\overline{u}^2}\right) \quad (1)$$

Where f = friction factor; h_f = head loss; L = pipe length; and g = acceleration attributable to gravity.

Concentration measurements were performed under 21 steady flow conditions with 5 replicates, covering Reynolds numbers ranging from 700 to 11,000. The valve was opened to the required discharge at the beginning of each test, and to ensure the flow was stable, a 0.5 s duration tracer injection was made 20 s after the test started. The data was recorded for between 60 and 600 s, depending on the design Reynolds number. Data for discharge and fluorometer concentration were

collected at 100 Hz. PLIF images were collected at different frequencies, ranging from 10 Hz to 100 Hz, to optimise storage space on the computer.

A specific accelerating flow condition was achieved by opening the digital control valve in multiple short steps. Initially, the valve was opened to achieve a design flow of Re = 1,000, which was maintained for 20 seconds before the acceleration began. The tracer injection took place for 0.5 s at the start of acceleration. Subsequently, the valve was gradually opened in multiple steps at 0.1s intervals, leading to an effective linear increase in the discharge Reynolds number to 10,500 over 18 seconds. Details on the valve operation during the accelerating flow can be found in Supplementary Material C. This acceleration rate was designed to be similar to the lowest acceleration rate (from Re = 2,700 to Re = 47,000 in 60 seconds) employed by Hart *et al.* (2021), which exhibited disaggregation in temporal concentration profiles. The flow was maintained at Re = 10,500 for 30 s until the tracer completely passed all the measurement locations. Ten repeats were conducted with the accelerating flow condition, and all data were logged at a frequency of 100 Hz.

As the fluorometers were significantly influenced by the laser in the PLIF units, measurements with fluorometers and PLIF were conducted separately.

Uniformity Index

PLIF provides the cross-sectional concentration distribution of the tracer. To quantify the degree of cross-sectional mixing within the recorded distribution, a Uniformity Index (*UI*) for the radial mean concentration distribution was calculated from the corrected and calibrated PLIF images.

In this study, the 24 mm diameter pipe area was discretised into 48 circles at 0.25 mm intervals. For each interval, the radial mean concentration, $c_m(r)$, was calculated from all the pixels between adjacent circles, using $c_m(r) = \sum c(r)/N$, where $c(r)$ is the individual pixel concentration and N is the number of pixels within the discretised area. The uniformity of this radial distribution was quantified using a *UI*, which correlates the radial mean concentration profile, $c_m(r)$, with the area

mean concentration, $\overline{c_m(r)}$. This *UI* (Eq. 2) is insensitive to the absolute value of concentration and the degree of discretisation

$$UI = 1 - \frac{\sum(c_m(r) - \overline{c_m(r)})^2}{\sum c_m(r)^2} \quad (2)$$

For a perfectly uniform concentration distribution, the *UI* is 1.0. However, perfect uniformity is not achievable under experimental conditions. To obtain a realistic value of the *UI* for well-mixed conditions in the experiments, the maximum *UI* was calculated using the images taken during calibration (where the tracer was believed to be well-mixed) for each PLIF unit. These were found to be > 0.997 for all four units. Any value of the *UI* less than the well-mixed *UI* indicates a cross-sectionally non-uniform condition and, the lower the value, the less uniform the distribution. Further details on the *UI* for ideal synthetic concentration distributions can be found in Supplementary Material D.

RESULTS

Pipe Hydraulics

Fig. 3(a) presents the relationship between the measured Head Loss and Reynolds number under steady flow conditions. The maximum headloss observed over the 11.8 m pipe is approximately 120 mm at Re = 11,000, indicating a smooth pipe system. Fig. 3(b) displays the resulting friction factor obtained using Eq.1. The analysis, based on standard laminar/turbulent pipe flow theory, indicates that the flow is laminar for Re < 2,300, turbulent for Re > 3,000, and transitional flow between.

Insert Fig. 3.

Steady Flows

Cross-sectional mean measurement

Fig. 4(a) presents examples of the measurements captured by the fluorometers, and Fig. 4(b) shows the cross-sectional area mean concentration derived from PLIF images under turbulent flow

conditions. The shaded red area represents the tracer injection, and the corresponding Reynolds number determined during the test is presented on the secondary y-axis. The measurements from fluorometers and PLIF were independent tests, leading to a minor discrepancy in the mean Reynolds number. However, the Reynolds number was maintained at around 10,400 during both tests. The spike observed in the Reynolds number during the injection phase is attributed to the pressure variation within the pipe.

Regarding the concentration profiles, the PLIF profiles are smoother compared to those of the fluorometers. Despite the fluorometer data being collected at a rate of 100 Hz, the physical measurement process within the fluorometers lacks a rapid response (i.e. at 33 HZ). The concentration profiles from both the fluorometers and PLIF share a characteristic slightly skewed Gaussian 'distribution', with decreasing peak concentrations and increasing spread with distance along the pipe.

Given that the fluorometers are situated upstream of the PLIF units, it was expected that the fluorometers would yield higher peak concentrations compared to PLIF. This trend is evident for the first three measurement locations. For the fourth fluorometer (F4), the fluorometer measurement reads 4 ppb while the area mean concentration from PLIF registers at 7 ppb. Despite the fluorometer measurements not confirming mass balance, the shape of the temporal profiles was captured by both instruments and the estimated longitudinal dispersion coefficient is consistent.

Similar results were obtained across the range of tests conducted under turbulent flow conditions. In light of this consistency, it is inferred that the fluorometers deliver a reliable measurement of the area mean concentration in turbulent flow conditions from which the longitudinal dispersion can be quantified from the method of moment.

Fig. 4(c) and (d) present the results from fluorometers and PLIF under a condition close to transitional flow (i.e. Re ≈ 3500). It should be noted that for better a representation of the concentration profiles, the ranges of the y-axis for the two subplots are different. Despite the fluorometers registering a

higher area mean concentration than PLIF, the shape of the concentration profiles measured by both instruments is quite consistent.

Fig. 4(e) and (f) present the results from fluorometers and PLIF under laminar flow conditions. It should be noted that for better a representation of the concentration profiles, the ranges of the y-axis for the two subplots are different. The Reynolds number was maintained steady during both tests and, as the pressure in the pipe was close to the injection pressure, the sudden increase in Reynolds number due to injection was not visible. It is notable that under this laminar flow condition, there is a substantial disagreement in the area mean concentration measurements between the fluorometers and PLIF. The fluorometers consistently reported much higher concentrations. For instance, F2 recorded a peak concentration of 23 ppb, while the area mean concentration derived from PLIF1 yielded a peak concentration of only 8 ppb.

This pattern of fluorometers reporting higher concentrations was found consistently across all the laminar flow conditions. This discrepancy might be attributed to the fact that when the tracer is not cross-sectionally well-mixed, the fluorometers do not account for the optical bias. The shape of the temporal concentration profiles measured by the PLIF was, as expected, non-Gaussian and unlike the fluorometers, the PLIF technique was able to capture the elongated tails. Overall, the comparison with the area mean concentration derived from PLIF images suggests that fluorometers do not provide a representative measurement of the cross-sectional area mean concentration under laminar flow conditions.

The shape of the temporal concentration profiles is more skewed and spread at low Reynolds numbers and it becomes less spread and close to a Gaussian form with the increase of Reynolds number.

Insert Fig. 4.

Cross-sectional concentration distribution

Fig. 5(a) shows the cross-sectional concentration distribution at selected times measured at the four PLIF locations in turbulent flow (Re = 10,408). The shade of red reflects the tracer concentration, but it should be noted that the range decreases from upstream locations to downstream locations due to the effects of longitudinal dispersion. The black circle indicates the 24 mm diameter pipe boundary. The three selected times in Fig. 5(a) correspond to the time when the tracer arrived at the measurement locations; the peak area mean concentration; and after the majority of the tracer had passed the measurement locations. The plots in the same row are from the same measurement location.

The effect of shear stress at the pipe boundary was evident at all the locations for this flow condition. As the tracer arrives, the concentration is primarily at the centre of the pipe, but as the tracer passes through, higher tracer concentration becomes prominent at the pipe boundary. The tracer is cross-sectionally well-mixed at all the measurement locations and it is almost uniformly distributed at the area mean concentration peaks, which indicates a high level of radial mixing.

Fig. 5(b) presents the corresponding temporal profiles for the uniformity index of the same test. The horizontal line on the y-axis is the lowest uniformity index calculated from the calibration images and is considered the uniformity index corresponding to well-mixed conditions. The shaded area is the area mean concentration (secondary y-axis), and the three vertical lines correspond to the three selected times shown in Fig. 5(a).

The uniformity index for the three selected times is consistent with the distributions shown in Fig. 5(a), demonstrating a more uniform distribution at the area mean concentration peaks (i.e. achieving a well-mixed condition at all the locations at peaks). The temporal uniformity index profiles at the four locations exhibit a trend of increasing with area mean concentration and maintaining a high value during the majority of the time of tracer passing, before decreasing towards the tail of the profile. The

tracer reached a condition, being cross-sectionally well-mixed (e.g. $UI > 0.95$), at all the measurement locations during the test and was better mixed at the downstream locations. PLIF1 and PLIF2 recorded 26.15% and 40.18 % of the test duration at the well-mixed condition, and PLIF3 and PLIF4 recorded 55.46% and 72.51%. These results confirm that it is not possible to have complete cross-sectional mixing throughout the complete duration of a tracer cloud, as the leading and trailing edges will always exhibit aspects of the longitudinal velocity profile, even under turbulent flow conditions.

Insert Fig. 5.

Fig. 6(a) presents the cross-sectional concentration distribution for the laminar flow condition (Re = 822). At the first measurement location (PLIF1), a clear progression of the tracer distribution is presented from a concentrated patch in the pipe centre gradually spreading out to form an annular shape extending towards the pipe edges. This trend is also evident at all downstream locations, but as the tracer is slightly more dense than the water, the cloud moves vertically downwards with distance along the pipe. The tracer distribution at laminar flow conditions presented in Fig. 6(a) is caused by the velocity distribution in the pipe, in which the tracer in the pipe centre travelled faster than the tracer near the pipe boundary, combined with very little radial mixing. Over this short distance (e.g. 5.5 m), the tracer is not cross-sectionally well-mixed (e.g. $UI < 0.6$), as shown by the corresponding uniformity index profiles, Fig. 6(b).

Across all four measurement locations, there was a consistent trend in the uniformity index. In the case of PLIF1, the uniformity index exhibited an increase towards the tail end of the concentration profiles, primarily influenced by background noise levels at low concentrations. At PLIF3 and PLIF4, a minor secondary peak in the uniformity index was evident. This observation may be attributed to the asymmetrical shape of the tracer concentration and the fact that the centre of the tracer patch is not aligned with the pipe's centre. It is important to note that the uniformity index does not define the shape of the concentration distribution: there are instances where uniformity index values are

identical, but the shape of the distribution is different. However, the uniformity index does serve as an indicator of how well the tracer is cross-sectionally mixed.

In laminar flow, the radial mixing is dominated by molecular diffusion, around 10^{-10} m^2/s, which requires long travel times to achieve fully mixed conditions. The non-uniform distributions also caused inaccurate measurement of area mean concentrations from the Fluorometers. Fluorometers are designed to measure only the areas containing tracer; at this condition, due to a large proportion of the pipe cross-section not containing tracer, the fluorometers do not accurately measure area mean concentration, and this led to the significantly elevated area mean concentrations in the fluorometers as shown in Fig. 4(c).

Insert Fig. 6.

Fig. 7 shows the uniformity index at the peak area mean concentration for all the steady flow conditions. It is evident that at laminar flow conditions (e.g. Re < 2,300), *UI* at the peak concentration is notably low (i.e. $UI_{peak} < 0.8$), which indicates poor radial mixing. However, as the Reynolds number increases, UI_{peak} increases, approaching well-mixed conditions and suggesting greater radial mixing. At transitional and turbulent flow conditions (Re > 2,300), the uniformity index for PLIF4 is closer to the well-mixed uniformity index than the upstream locations. This indicates that well-mixed conditions did not occur instantaneously, but the tracer became more uniformly distributed as it travelled downstream.

Insert Fig. 7.

Accelerating Flow

Cross-sectional mean measurement

Fig. 8(a) shows the measurements from the fluorometers during the accelerating flow, with the secondary y-axis showing the measured Reynolds number during the test. In this test, the flow was accelerated linearly from Re = 1,200 to Re = 10,000 between 20 s and 38 s, with the tracer injection at the start of the acceleration. The measured temporal concentration profiles at all four locations showed two peaks, with the concentration at the first peak being higher than the second. Due to dispersion effects, the downstream peaks are lower and the distribution exhibits a greater spread.

Fig. 8(b) shows the derived cross-sectional area mean concentration profiles from the PLIF images for an identical accelerating flow test. Area mean PLIF distributions also exhibited two peaks at all the locations, but the area mean concentration was less than half the values given by the fluorometers (e.g. 15 ppb versus 42 ppb at the first measurement location). This indicates that the non-uniform concentration distribution experienced in the laminar flow conditions also influenced the accuracy of the fluorometer measurements during accelerating flow. At downstream locations, the temporal separation between the two peaks is more distinct, suggesting that the tracer contributing to the first peak was travelling faster than the second and the differential velocity between the peaks increased.

The temporal concentration profiles exhibited two peaks in all 10 repeat tests under the accelerating flow conditions, which is consistent with the findings of Hart *et al*. (2021). It should be noted that in this study two peaks were consistently observed from all the PLIF measurements, even at the first measurement location, and the disaggregation from a single upstream peak to downstream multiple peaks was not evident in the PLIF data. This can be attributed to the differences from Hart *et al*. (2021) in both the initial Reynolds number and the distance from the injection point to the first measurement location. The initial Reynolds number in this study was around 1,200, lower than the 2,700 used by Hart *et al*. (2021). A lower initial Reynolds number implies that the distance to detect the effects of

differential longitudinal advection is shorter and in the current work the closest PLIF was 0.834 m from the injection point in comparison to the 0.5 m from the injection point in Hart *et al*. (2021).

The shaded blue area in Fig. 8(a) and (b) is the region where the mean flow measured for steady flow conditions was within the transitional flow regime. By the time the tracer reached the first PLIF measurement location (PLIF1, around 25 s), the flow within the pipe was turbulent.

Insert Fig. 8.

Cross-sectional concentration distribution

Fig. 9(a) illustrates the cross-sectional concentration distribution at four PLIF measurement locations during the accelerating flow. The selected times correspond to when the area mean concentration reached its first peak, its second peak, and one instance between the two peaks.

At PLIF1, the first peak showed a cross-sectional distribution that was not well-mixed with the tracer concentrated primarily in the central region of the pipe. At the second peak, the tracer reached the pipe boundary accompanied by eddies in the central area. Between the two peaks at t = 28.01 s, the concentration distribution took on an annular shape near the pipe boundary, similar to the distribution seen in the late-stage of laminar flows. At PLIF2 and PLIF3, similar concentration distributions were recorded. However, at PLIF4, the tracer exhibited a uniform, well-mixed cross-sectional distribution throughout the duration of the tracer.

The concentration distribution provides insights into the behaviour of the tracer during the accelerating flow. The tracer located in the pipe centre contributes to the first peak of the temporal profile; the tracer located at pipe boundary contributes to the second peak. The tracer becomes cross-sectionally well-mixed due to rapid radial mixing during turbulent flow conditions. Due to the velocity distribution within the pipe and the acceleration of the flow, the tracer in the pipe's central region accelerates more rapidly than the tracer at the pipe's boundary, leading to a greater separation

between the two peaks at downstream locations, as shown in the area mean temporal concentration profiles in Fig. 8(b).

Fig. 9(b) is the temporal profile of the *UI* with vertical lines indicating the selected times in Fig. 9(a); Table 1 summarises the conditions of the two peaks presented in Fig. 8(b).

Insert Table 1.

An interesting observation is that, despite the mean flow in the pipe being turbulent (Re = 4,626) when the tracer arrived at the first measurement location at 26.12 s, the tracer was not cross-sectionally well-mixed. It wasn't until around 37.31 s (Re = 10,147) at PLIF4, that the first patch of tracer became cross-sectionally well-mixed, whilst the second patch of tracer was cross-sectionally well-mixed at PLIF2 at 31.34 s (Re = 7,404). This phenomenon may be attributed to spatial velocity development and cross-sectional velocity distributions. Whilst the mean flow exhibited rapid acceleration due to the valve opening, it remains uncertain whether this acceleration happened simultaneously at all locations within the pipe. A delayed change to turbulent flow conditions at downstream locations could result in non-uniform cross-sectional tracer distributions, despite the mean discharge from the pipe suggesting fully turbulent flow conditions. The first cloud of tracer is located at the pipe centre and to achieve cross-sectional well-mixed conditions requires sufficient radial mixing. Under accelerating flows, the radial velocity gradient towards the centre of the pipe may not increase sufficiently for this to occur. However, the second cloud of tracer is located close to the pipe boundary, and this tracer attains cross-sectionally well-mixed conditions at an earlier stage of acceleration from higher radial mixing caused by greater velocity gradients at the boundary. Clearly, detailed spatial and temporal velocity measurements are needed to confirm this hypothesis.

Insert Fig. 9.

DISCUSSION

The comparison between fluorometer and PLIF measurements highlighted a significant limitation, specifically during laminar flow conditions, when the tracer in the pipe was not uniformly mixed across the pipe cross-section. Under such flows, the fluorometers did not yield reliable measurements of the cross-sectional area mean concentration. This suggests that the method of sampling tracer during laminar flow can significantly impact the accuracy of experimental data and subsequent determination of longitudinal dispersion coefficients. The measured concentration from fluorometers at laminar flows, e.g. in Hart *et al*. (2016), may not be representative of pipe cross-sectional mean concentration. In some studies (Piazza *et al*., 2020, & 2022; Romero-Gomez and Choi, 2011) where the tracer was sampled at the pipe wall, it may lead to an inaccurate representation of tracer concentration during laminar flow.

The influence of the sampling method extends to applications involving water quality analysis (e.g. inorganics, disinfectant and biofilm) in the main water distribution network (e.g. Abokifa *et al*. 2016; Prévost *et al*. 1997). Evaluating the representativeness of collected data, particularly during low flows, requires careful consideration of the degree of cross-sectional mixing. This factor becomes critical in determining the accuracy and reliability of water quality assessments derived from sampled data within the distribution network.

PLIF measurements offer a more accurate representation of the pipe's cross-sectional mean concentration than single-point sampling. However, implementing this technique in live water distribution networks may be unfeasible. Nonetheless, the PLIF data collected in this study holds substantial value for the broader community within the field, providing valuable insights into pipe cross-sectional concentration distributions and area mean concentration that can guide future research and development in this area.

EPANET has long been used to study hydraulics and water quality in water distribution systems. The inclusion of dispersion effects in the conventional advection-based EPANET model has proven to

improve its predictions, as evidenced by comparisons between modelled and experimentally measured data (Burkhardt *et al*. 2020; Piazza *et al*. 2020, 2022; Shang *et al*. 2023). The refinement of numerical models often relies on experimental data to verify model accuracy. In this context, the PLIF dataset gathered in this study serves as a source of pipe cross-sectional mean concentration data, facilitating further validation of the 1D model. Additionally, the cross-sectional concentration distribution offers an opportunity for extended validation of 2D models which are essential to describe contaminant interactions with boundary biofilms and pipe material.

CONCLUSIONS

Four fluorometers and PLIF units were used to measure the cross-sectional area mean temporal concentration profiles resulting from a single pulse of tracer injected at an upstream location under steady and accelerating flows. Observations in steady turbulent flows showed that the fluorometers deliver a reliable measurement of the area mean concentration. However, due to low radial mixing, the fluorometers do not offer an accurate measurement of the cross-sectional area mean concentration under laminar flow conditions.

PLIF provides, for the first time, the opportunity for visualisation of pipe cross-sectional tracer concentration distribution development and evolution due to radial mixing at different steady flow conditions. It showed that the tracer is cross-sectionally well-mixed at all the measurement locations in turbulent flows. In laminar flows, a clear progression was observed with an initial distribution at the pipe centre, gradually spreading to form an annular shape extending towards the pipe wall. This is a result of the velocity distribution and the low radial mixing.

In the accelerating flow condition, the temporal concentration profiles measured at all the downstream locations showed two peaks with the first peak being higher than the second. The cross-sectional PLIF concentration distributions revealed that at the first measurement location, the two peaks were not cross-sectionally well-mixed, but at a downstream location, the two peaks became

cross-sectionally well-mixed. This provides a significant improvement in understanding the temporal and spatial variations in radial mixing during accelerating pipe flows.

The disaggregation from a single upstream peak to downstream multiple peaks was observed in this study and is consistent with the observations of Hart et al. (2021). The new cross-sectional PLIF data provided the opportunity to quantify the difference in the spatial distribution of the tracer at the peaks for the first time. The cause of the disaggregation requires detailed velocity measurements to identify the underlying mechanisms.

Evaluating the representativeness of collected data, particularly during low flows and where the water sample is taken from a single point at the pipe wall, requires careful consideration of the degree of cross-sectional uniformity. The PLIF data collected in this study provides an accurate representative measurement of pipe cross-sectional mean concentration and holds substantial value for model validations.

DATA AVAILABILITY STATEMENT

The data, models, and code generated or used during the study are available in a repository or online in accordance with funder data retention policies from Peng *et al*. (2024) (https://doi.org/10.15131/shef.data.23735919).

ACKNOWLEDGEMENTS

The authors would like to thank Joseph Milner, who provided technical support for all the laboratory studies conducted at the University of Sheffield. Additional appreciation was also given to Professor Shuisheng He and Oliver Cooper for their generous provision and assistance in using their lab space. This work was supported by the EPSRC Grant No. EP/P012027/1.

SUPPLEMENTARY MATERIALS

Supplementary Materials A, B and C are available online in the ASCE Library (ascelibrary.org).

REFERENCE

Abokifa, A. A., Yang, Y. J., Lo, C. S., and Biswas, P. (2016). "Water quality modeling in the dead end sections of drinking water distribution networks." *Water Research*, Pergamon, 89, 107–117.

Buchberger, S. G., Carter, J. T., Lee, Y., and Schade, T. G. (2003). "Random demands, travel times and water quality in deadends." *Rep. No. 90963F:470*, Denver: American Water Works Association Foundation.

Burkhardt, J. B., Woo, H., Mason, J., Shang, F., Triantafyllidou, S., Schock, M. R., Lytle, D., and Murray, R. (2020). "Framework for Modeling Lead in Premise Plumbing Systems Using EPANET." *Journal of Water Resources Planning and Management*, American Society of Civil Engineers (ASCE), 146(12), 04020094.

Crimaldi, J. P. (2008). "Planar laser induced fluorescence in aqueous flows." *Experiments in Fluids*, Springer, 44(6), 851–863.

Fischer, H. B., List, J. E., Koh, C. R., Imberger, J., and Brooks, N. H. (1979). *Mixing in Inland and Coastal Waters*. Elsevier.

Flint, L. F., and Eisenklam, P. (1969). "Longitudinal gas dispersion in transitional and turbulent flow through a straight tube." *The Canadian Journal of Chemical Engineering*, John Wiley & Sons, Ltd, 47(2), 101–106.

Fowler, F. C., and Brown, G. G. (1943). *Contamination by Successive Flow in Pipe Lines*. American institute of chemical engineers.

Greenblatt, D., and Moss, E. A. (2004). "Rapid temporal acceleration of a turbulent pipe flow." *Journal of Fluid Mechanics*, Cambridge University Press, 514, 65–75.

Harry, A.J., Pearson, J.M., Guymer, I. and Potter, R., (1996). "Development of an In-situ

516 Concentration Measurement Technique to Investigate Vertical Mixing Processes in the Coastal
517 Zone." *Proceedings of Second International Conference on Hydrodynamics*, Hong Kong, 16-19
518 December, 1007–1012.

519 Hart, J. R., Guymer, I., Sonnenwald, F., and Stovin, V. R. (2016). “Residence Time Distributions for
520 Turbulent, Critical, and Laminar Pipe Flow.” *Journal of Hydraulic Engineering*, 142(9), 1–10.

521 Hart, J., Sonnenwald, F., Stovin, V., and Guymer, I. (2021). “Longitudinal Dispersion in Unsteady Pipe
522 Flows.” *Journal of Hydraulic Engineering*, 147(9), 1–12.

523 He, S., and Jackson, J. D. (2000). “A study of turbulence under conditions of transient flow in a pipe.”
524 *Journal of Fluid Mechanics*, Cambridge University Press, 408, 1–38.

525 Keyes, J. J. (1955). “Diffusional film characteristics in turbulent flow: Dynamic response method.”
526 *AIChE Journal*, John Wiley & Sons, Ltd, 1(3), 305–311.

527 Kurokawa, J., and Morikawa, M. (1986). “Accelerated and Decelerated Flows in a Circular Pipe : 1st
528 Report, Velocity Profile and Friction Coefficient.” *Bulletin of JSME*, The Japan Society of
529 Mechanical Engineers, 29(249), 758–765.

530 Lee, J., Burkhart, J.B., Buchberger, S., Grayman, W., Haxton, T, Janke, R., Murray, R. and Platten, W.E.
531 (2023). “*Premise Plumbing Modeling*.” ASCE, Env. & Water Resources Institute.

532 LeChevallier, M. W., Gullick, R. W., Karim, M. R., Friedman, M., and Funk, J. E. (2003). “The potential
533 for health risks from intrusion of contaminants into the distribution system from pressure
534 transients.” *Journal of Water and Health*, IWA Publishing, 1(1), 3–14.

535 Mathieu, J., and Scott, J. (2000). *An introduction to turbulent flow*. Cambridge University Press.

536 Peng, Z., Stovin, V., and Guymer, I. (2024). “Cross-sectional solute concentration distribution in
537 steady and accelerating pipe flows”. The University of Sheffield, 10.15131/shef.data.23735919.

538 Piazza, S., Mirjam Blokker, E. J., Freni, G., Puleo, V., and Sambito, M. (2020). “Impact of diffusion and
539 dispersion of contaminants in water distribution networks modelling and monitoring.” *Water*

Supply, IWA Publishing, 20(1), 46–58.

Piazza, S., Sambito, M., and Freni, G. (2022). "A Novel EPANET Integration for the Diffusive–Dispersive Transport of Contaminants." *Water 2022, Vol. 14, Page 2707*, Multidisciplinary Digital Publishing Institute, 14(17), 2707.

Prévost, M., Rompré, A., Baribeau, H., Coallier, J., and Lafrance, P. (1997). "Service lines: Their effect on microbiological quality." *Journal - American Water Works Association*, American Water Works Association, 89(7), 78–91.

Romero-Gomez, P., and Choi, C. Y. (2011). "Axial Dispersion Coefficients in Laminar Flows of Water-Distribution Systems." *Journal of Hydraulic Engineering*, American Society of Civil Engineers, 137(11), 1500–1508.

Rossman, L. A. 2000. EPANET 2: Users manual. Washington, DC: USEPA

Shang, F., Burkhardt, J. B., and Murray, R. (2023). "Random Walk Particle Tracking to Model Dispersion in Steady Laminar and Turbulent Pipe Flow." *Journal of Hydraulic Engineering*, 149(7), 1–9.

Swarnkar, K., Nikam, V., Gupta, K., and Pearson, J. M. (2022). "Review of the state-of-the-art for monitoring urban drainage water quality using rhodamine WT dye as a tracer." *https://doi.org/10.1080/09715010.2022.2098682*, Taylor & Francis.

Taylor, G. I. (1954). "The dispersion of matter in turbulent flow through a pipe." *Proceedings of the Royal Society of London. Series A. Mathematical and Physical Sciences*, The Royal Society London, 223(1155), 446–468.

van Cruyningen, I., Lozano, A. and Hanson, R.K., (1990). "Quantitative Imaging of Concentration by Planar Laser Induced Fluorescence. " Experiments in Fluids, Vol. 10, pp 41-49.

Wilson, J. F., Cobb, E. D., and Kilpatrick, F. A. (1986). *Fluorometric procedures for dye tracing*. Department of the Interior, US Geological Survey.

Fig. 1. Disaggregation in accelerating flow (from Hart *et al*., 2021).

Fig. 2. Experimental set-up and instrumentation; (a) pipe test section (not to scale); (b) 2D PLIF unit (plan view); (c) Snapshot of food dye injection.

Fig. 3. Variation of (a) head loss and (b) friction factor with Reynolds number.

Fig. 4. Temporal concentration profiles at steady flow conditions; (a) measured by fluorometers at Re = 10,452; (b) area mean concentration profiles derived from 2D PLIF images at Re = 10,408; (c) measured by fluorometers at Re = 861; (d) area mean concentration profiles derived from 2D PLIF images at Re = 822.

Fig. 5. Steady flow condition at Re = 10,408; (a) cross-sectional concentration distribution for selected times; (b) temporal uniformity index profiles derived from PLIF images, the vertical lines correspond to the selected times in Fig. 4(a).

Fig. 6. Steady flow condition at Re = 822; (a) cross-sectional concentration distribution for selected times; (b) temporal uniformity index profiles derived from PLIF images (the vertical lines correspond to the selected times in Fig. 5(a)).

Fig. 7. Variation of uniformity index at peak area mean concentrations with Reynolds number.

Fig. 8. Temporal concentration profiles at the accelerating flow; (a) measured by fluorometers; (b) area mean concentration derived from 2D PLIF images.

Fig. 9. Accelerating flow condition; (a) cross-sectional concentration distribution for selected times; (b) temporal uniformity index profiles derived from PLIF images at the accelerating flow, the vertical lines correspond to the selected times in Fig. 8(a).

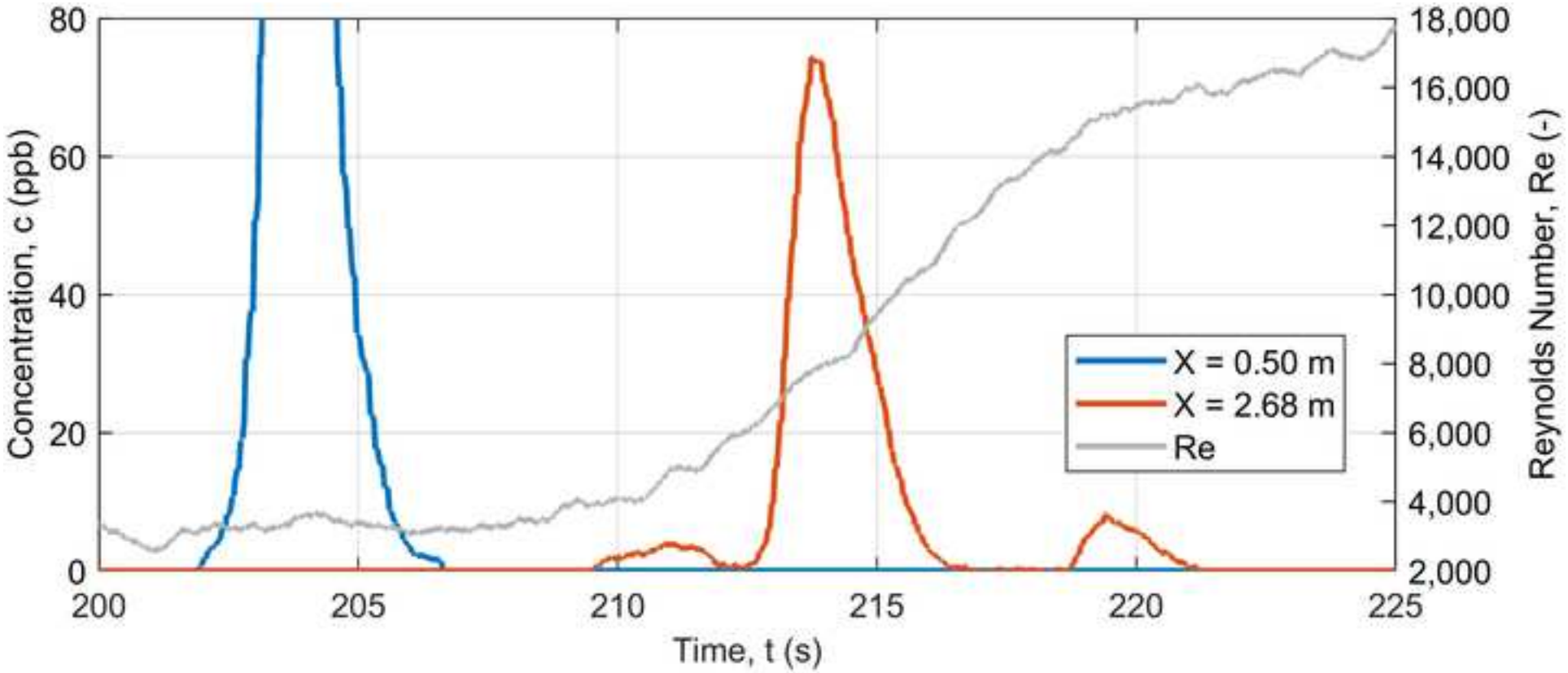
Concentration, c (ppb)
Reynolds Number, Re (-)
Time, t (s)
X = 0.50 m
X = 2.68 m
Re
0
20
40
60
80
2,000
4,000
6,000
8,000
10,000
12,000
14,000
16,000
18,000
200
205
210
215
220
225

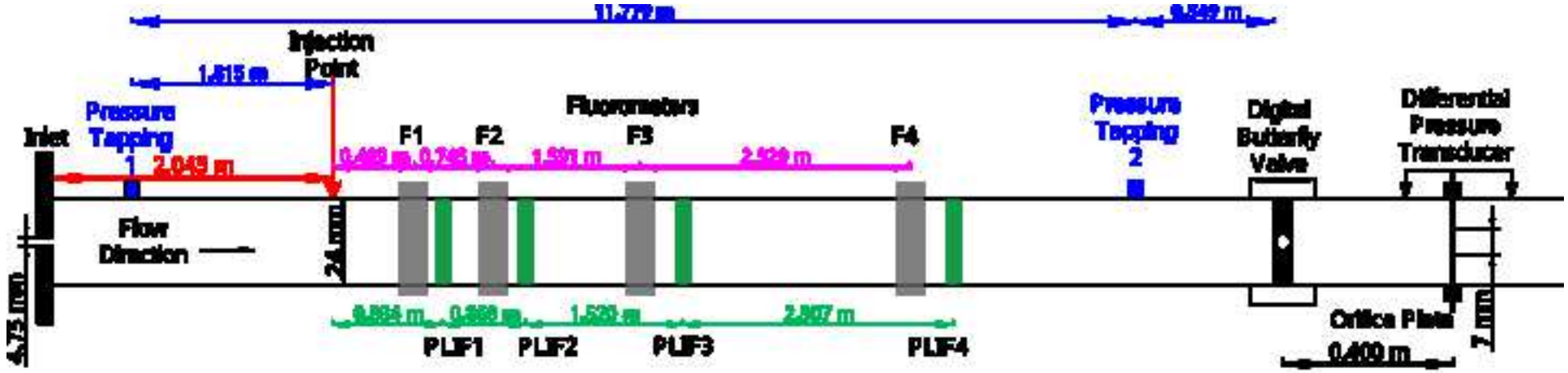
Injection Point
Pressure Tapping 1
Inlet
Flow Direction
Fluorometers
F1
F2
F3
F4
Pressure Tapping 2
Digital Butterfly Valve
Differential Pressure Transducer
PLIF1
PLIF2
PLIF3
PLIF4
Orifice Plate

(a)

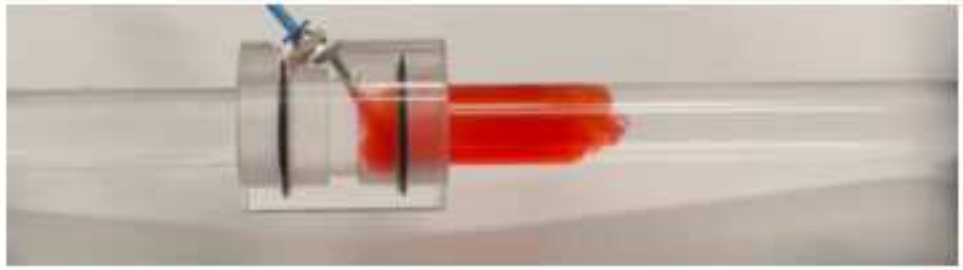

(b)

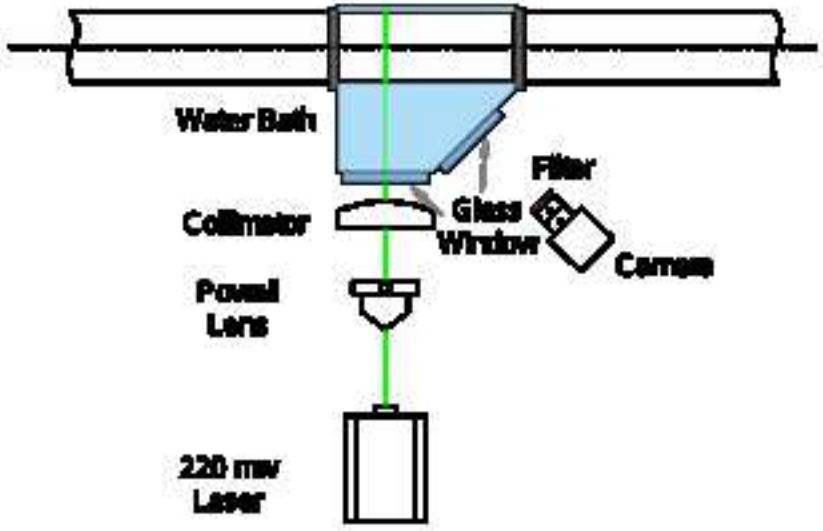
Water Bath
Filter
Collimator
Glass Window
Camera
Powell Lens
220 mw Laser

(c)

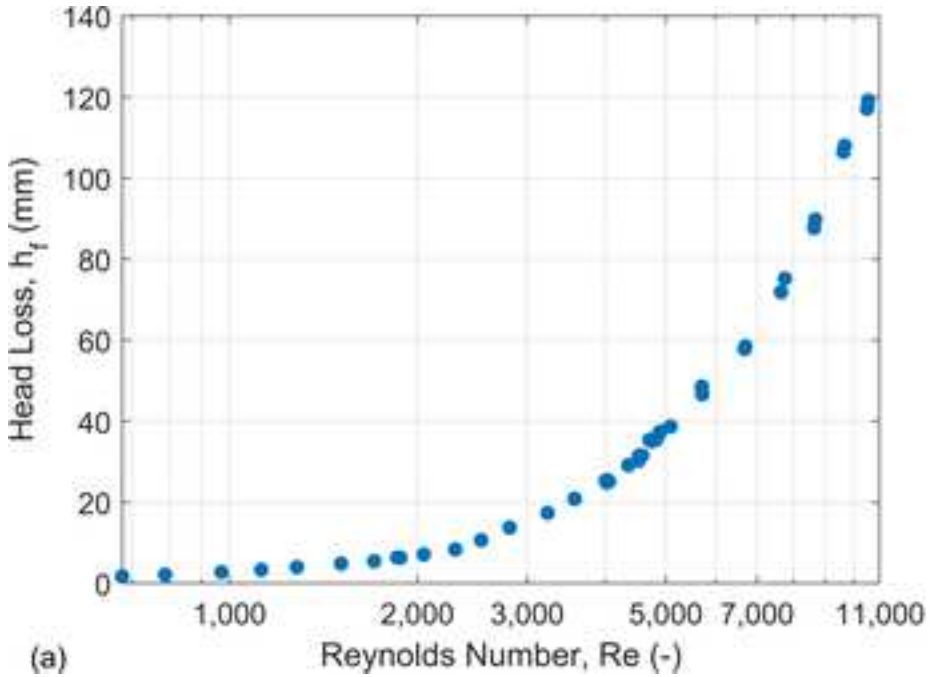
Head Loss, h_f (mm)
140
120
100
80
60
40
20
0
1,000
2,000
3,000
5,000
7,000
11,000
Reynolds Number, Re (-)

(a)

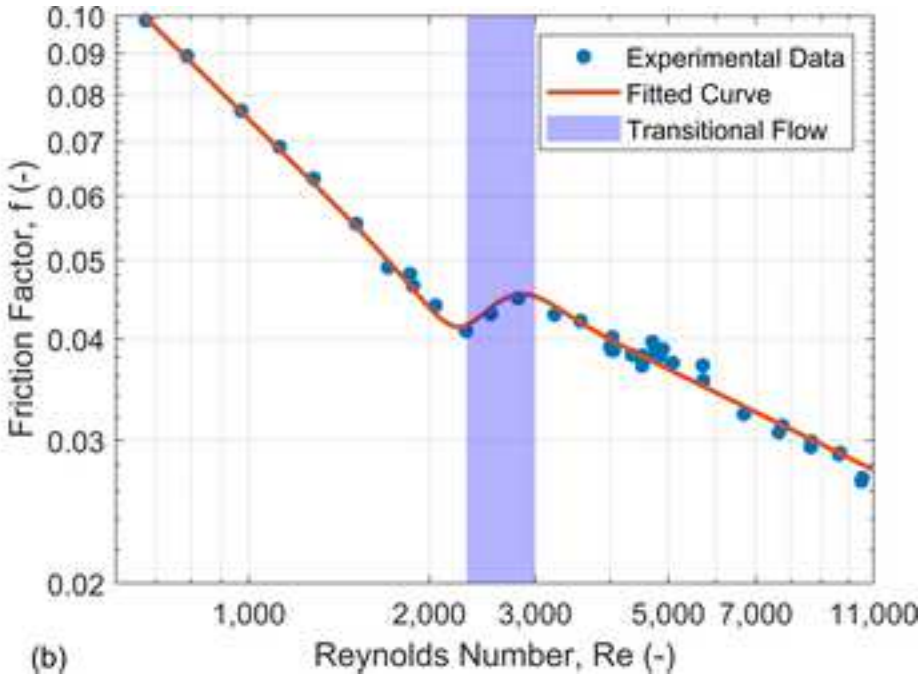
Friction Factor, f (-)
0.10
0.09
0.08
0.07
0.06
0.05
0.04
0.03
0.02
Experimental Data
Fitted Curve
Transitional Flow
1,000
2,000
3,000
5,000
7,000
11,000
Reynolds Number, Re (-)

(b)

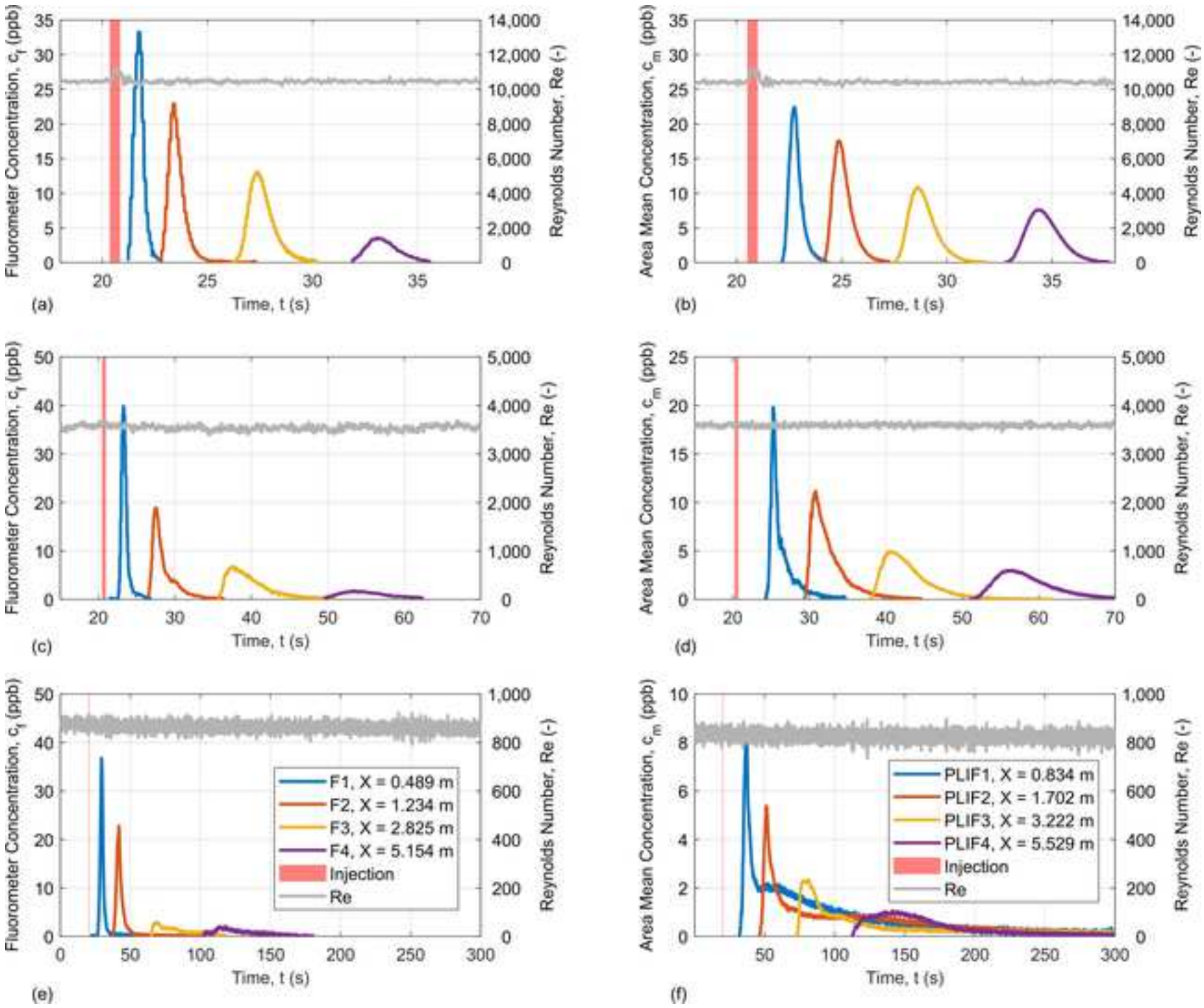
Fluorometer Concentration, c_f (ppb)
Area Mean Concentration, c_m (ppb)
Reynolds Number, Re (-)
Time, t (s)
(a)
(b)
(c)
(d)
(e)
(f)
F1, X = 0.489 m
F2, X = 1.234 m
F3, X = 2.825 m
F4, X = 5.154 m
Injection
Re
PLIF1, X = 0.834 m
PLIF2, X = 1.702 m
PLIF3, X = 3.222 m
PLIF4, X = 5.529 m

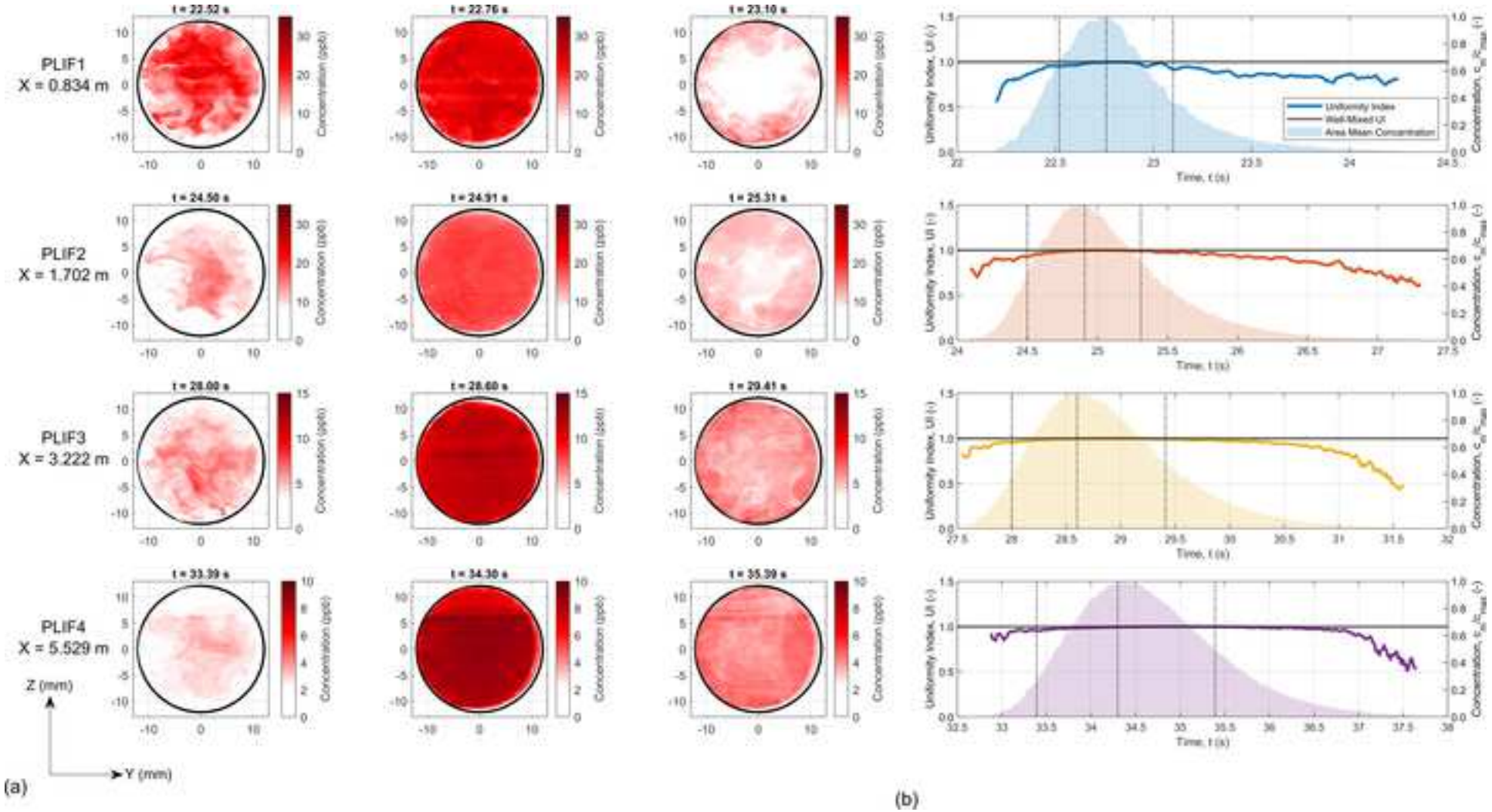
PLIF1
X = 0.834 m
PLIF2
X = 1.702 m
PLIF3
X = 3.222 m
PLIF4
X = 5.529 m
t = 22.52 s
t = 22.76 s
t = 23.10 s
t = 24.50 s
t = 24.91 s
t = 25.31 s
t = 28.00 s
t = 28.60 s
t = 29.41 s
t = 33.39 s
t = 34.30 s
t = 35.39 s
Concentration (ppb)
Z (mm)
Y (mm)
(a)
Uniformity Index
Well-Mixed UI
Area Mean Concentration
Uniformity Index, UI (-)
Concentration, c_m/c_max (-)
Time, t (s)
(b)

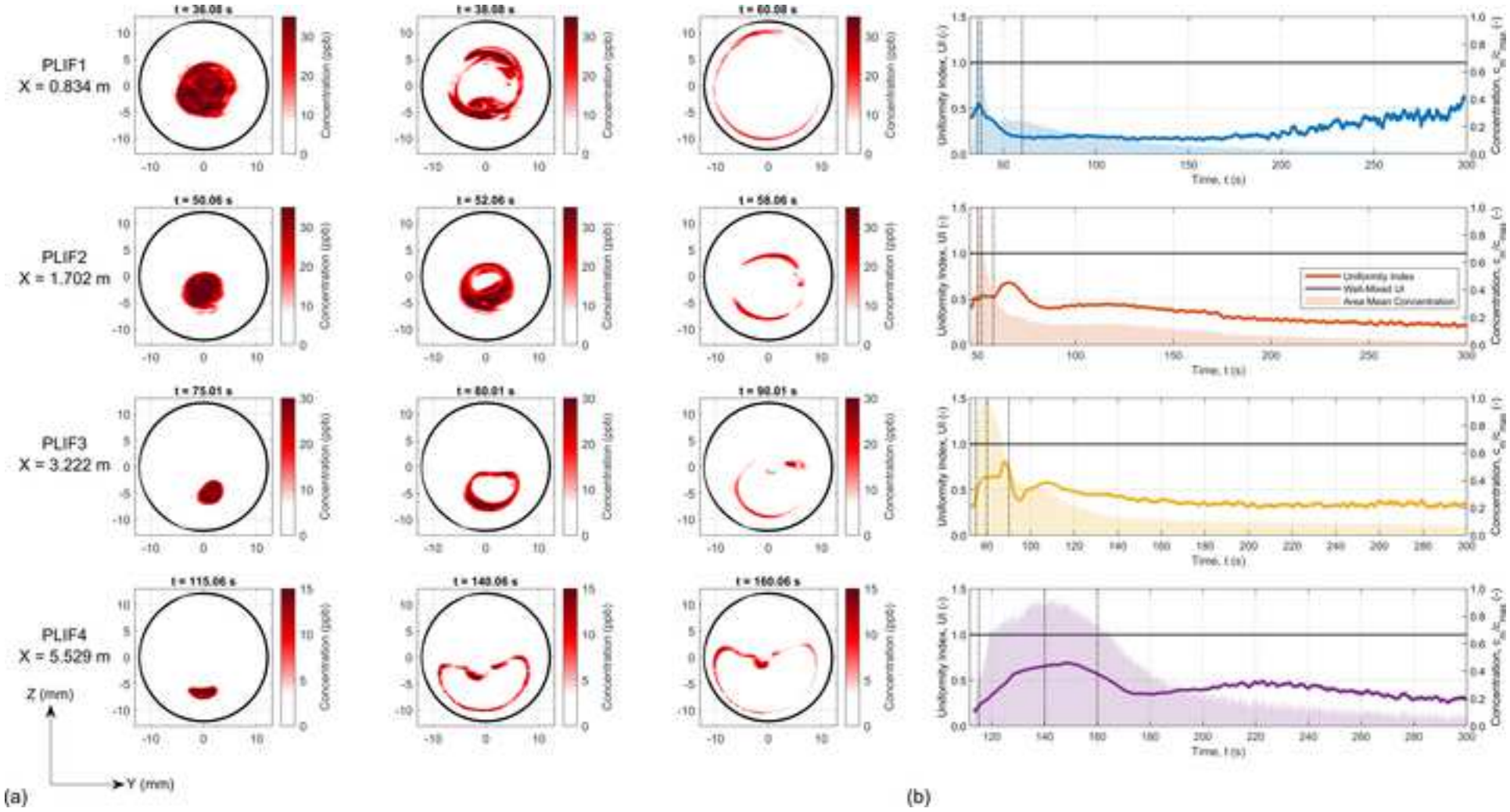
PLIF1
X = 0.834 m
PLIF2
X = 1.702 m
PLIF3
X = 3.222 m
PLIF4
X = 5.529 m
Z (mm)
Y (mm)
Concentration (ppb)
Uniformity Index
Well-Mixed UI
Area Mean Concentration
Time, t (s)
(a)
(b)

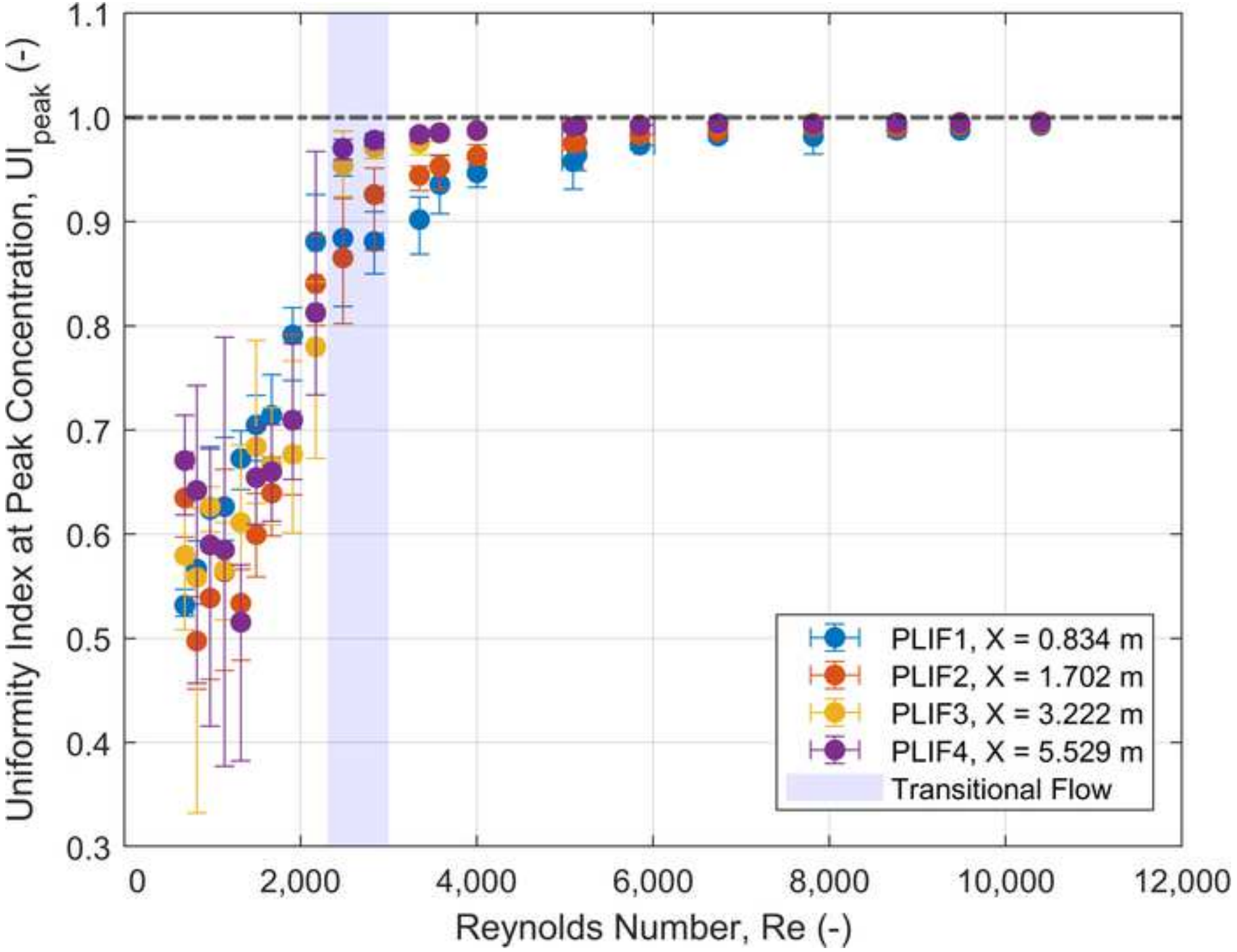
Uniformity Index at Peak Concentration, UI_{peak} (-)
1.1
1.0
0.9
0.8
0.7
0.6
0.5
0.4
0.3
0
2,000
4,000
6,000
8,000
10,000
12,000
Reynolds Number, Re (-)
PLIF1, X = 0.834 m
PLIF2, X = 1.702 m
PLIF3, X = 3.222 m
PLIF4, X = 5.529 m
Transitional Flow

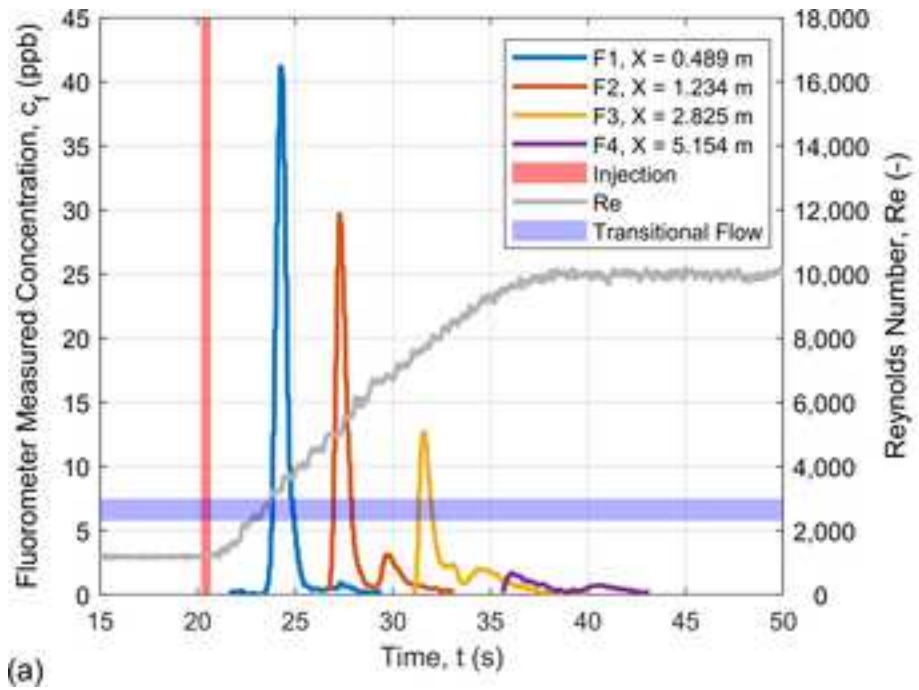
Fluorometer Measured Concentration, c_f (ppb)
Reynolds Number, Re (-)
Time, t (s)
F1, X = 0.489 m
F2, X = 1.234 m
F3, X = 2.825 m
F4, X = 5.154 m
Injection
Re
Transitional Flow
(a)

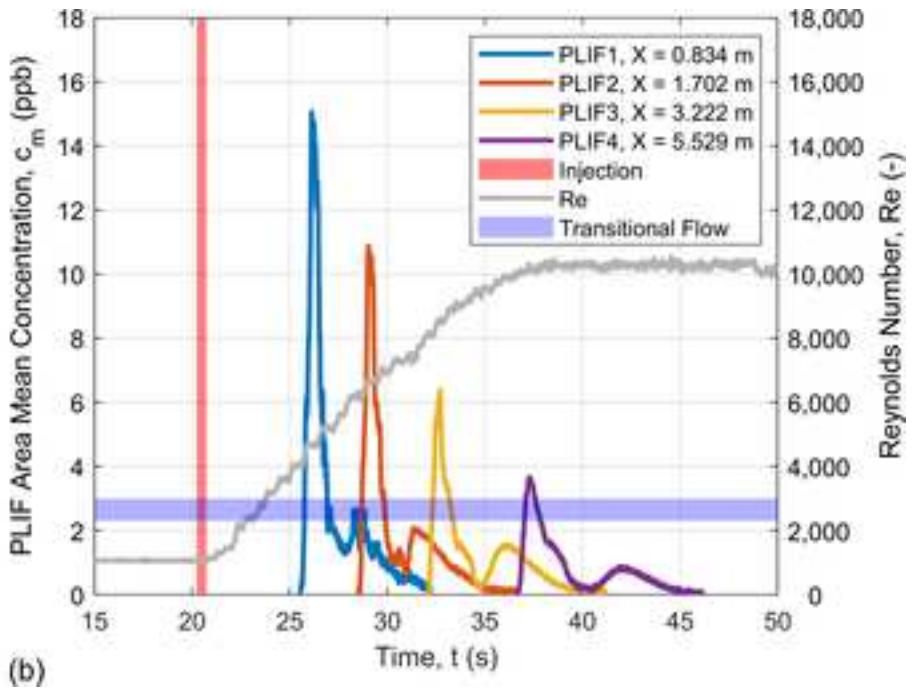
PLIF Area Mean Concentration, c_m (ppb)
Reynolds Number, Re (-)
Time, t (s)
PLIF1, X = 0.834 m
PLIF2, X = 1.702 m
PLIF3, X = 3.222 m
PLIF4, X = 5.529 m
Injection
Re
Transitional Flow
(b)

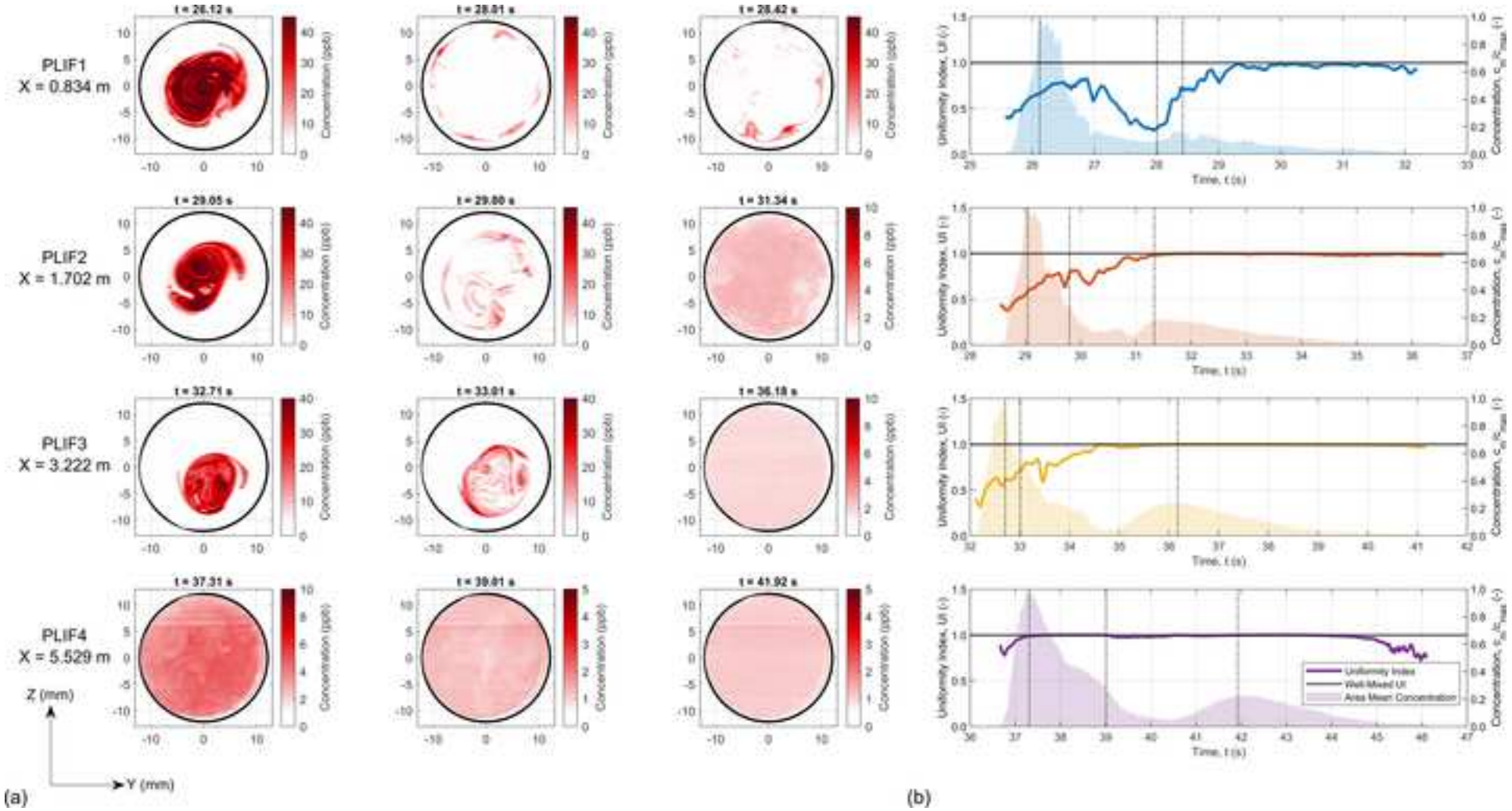
PLIF1
X = 0.834 m
PLIF2
X = 1.702 m
PLIF3
X = 3.222 m
PLIF4
X = 5.529 m
t = 26.12 s
t = 28.01 s
t = 28.62 s
t = 29.05 s
t = 29.80 s
t = 31.34 s
t = 32.71 s
t = 33.01 s
t = 36.18 s
t = 37.31 s
t = 39.01 s
t = 41.92 s
Concentration (ppb)
Uniformity index, UI (-)
Concentration, c_ai/c_max (-)
Time, t (s)
Uniformity Index
Well-Mixed UI
Area Mean Concentration
Z (mm)
Y (mm)
(a)
(b)